Tropical Forest Carbon Accounting through Deep Learning-Based Species Mapping And Tree Crown Delineation

Final Report

Georgia Ray[1]
[1] Imperial College London
GitHub: edsml-ger23
GitHub Repository: https://github.com/ese-msc-2023/irp-ger23
Email: georgia.ray23@imperial.ac.uk

Supervision by Minerva Singh and Adriana Paluszny

An Independent Research Project
Submitted to the Department of Earth Science and Engineering
Imperial College London
In Partial Fulfilment for the Requirements
For the Degree MSc Environmental Data Science and Machine Learning
August 23, 2024

Abstract

Tropical forests are essential ecosystems recognized for their carbon sequestration and biodiversity benefits. As the world undergoes a simultaneous data revolution and climate crisis, accurate data on the world's forests is increasingly important. The importance is particularly stark for burgeoning climate offset markets, reliant on accurate and verifiable estimates of carbon storage provided by afforestation or preventative deforestation. Traditional methods are often expensive and imprecise, relying on ground-based measurements and low-resolution satellite imagery, leading to an overestimation in accounted carbon.

Using the ReforesTree dataset (Reiersen et al., 2022), this project employs a single encoder, double decoder (SEDD) model to generate a species segmentation map, regularized by a distance map in training. Used alongside bounding box predictions from a fine-tuned version of the well-established DeepForest model (Weinstein et al., 2020), this study accurately predicts the location and species of 67% of trees in the dataset. For the two most common species, unincumbered by sparse data challenges, that metric is even higher at 84%. This efficient processing of aerial RGB imagery can then be used to predict carbon sequestration potential, made possible by a custom model for estimating Diameter at Breast Height (DBH) based on bounding box coordinates and species identification, and species-specific, custom allometric equations for Aboveground Biomass (AGB) prediction. Ultimately, the predicted carbon across the test set accounted for by the trees for which species was correctly predicted has a relative error of 2% compared to groundtruth carbon sequestration potential, a relative error much lower than those seen by previous carbon accounting strategies.

1. Introduction

Comprising the largest proportion of the world's forests, tropical forests play a crucial role as a carbon sink. Carbon is stored in forests via vegetation, soil, and litter (Sun and Liu, 2019), and over 70% of the global, vegetation-based carbon storage can be attributed to forests. 36% is attributed to tropical forests specifically (IPCC, 2022).

But deforestation, wildfires, and extreme weather threaten forests' future. Between 2010 and 2020, 4.7 million ha of forest land was lost per year, equating to a loss over the 10-year-period approximately equivalent to the whole of Kenya (FAO, 2020). This is particularly concerning because forests are essential not only for carbon storage but also for protecting against soil erosion, regulating the water cycle, and supporting local economic systems. Forests also provide a refuge for 80% of the world's land-based biodiversity (Shi et al., 2021).

Accurate carbon storage metrics in forests are imperative to monitoring forest health and ensuring transparency in carbon offset markets. Carbon offset credits are often based on preventative deforestation, meaning a reliable carbon storage baseline helps calculate the number of credits issued. For most projects the minimum baseline is the regional average carbon stock density for the forest type (Haya 2023). Current forest carbon stock practices systematically overestimate the amount of storage, up to a value of $410 million, a metric calculated in California alone (Badgley et al., 2022, Sun and Liu, 2019).

Additionally, most afforestation and deforestation is happening in low and middle income countries, necessitating scalable and cost-efficient methods for calculating carbon storage. Mapping forests with remote sensing data has proven cheaper and faster than traditional methods (Fassnacht et al., 2016) and developing methods using free or easily accessible images and technologies is an emerging focus in the field (Korznikov et al., 2021, Reiersen et al., 2022).

There is a strong body of research on Individual Tree Crown (ITC) delineation, not applied to carbon sequestration potential. Deep learning models, such as Faster R-CNN and Mask R-CNN, have shown promise. Braga et al. (2020) use an Instance Segmentation approach with Mask R-CNN in tropical forests while Wu et al. (2020) focus on apple orchards using Semantic Segmentation and convex boundary extraction. Weinstein et al. (2020) present DeepForest, a package specifically designed for ITC

delineation on RGB images, while Lassalle et al. (2022) show integrating deep learning models with advanced image processing techniques, such as watershed segmentation, can further enhance the accuracy of ITC.

Similarly, there is a significant body of research on tree species identification using deep learning. There has been research into 3D-CNNs for hyperspectral images (Zhang et al., 2020), a SVM classifier for a Mixed Ombrophilous Forest ecosystem (Sothe et al., 2019), and the integration of LiDAR data and multispectral imagery for enhanced species classification (Fassnacht et al., 2016). Korvnikov et al. (2021) demonstrated U-Net-like CNNs outperform traditional machine learning methods in pixel-based species segmentation using high-resolution RGB satellite images.

More recently, there has been a move towards a combined approach, training networks to identify species and perform ITC delineation simultaneously (La Rosa et al., 2021, Martins et al., 2021). In a tropical urban context, Martins et al. (2021) demonstrated CNNs can be trained to identify individual tree crowns and estimate their biomass using high-resolution RGB imagery. Ferreira et al. (2020) employed a deep learning model to detect individual trees and classify their species in UAV-RGB images, applying these techniques to large-scale forest monitoring.

Despite research into ITC delineation and species segmentation, there has been no work done, to this author's knowledge, to bring the fields together for application towards carbon accounting. When considering other approaches to estimating carbon, they have largely been regional. Spawn et al. (2020) use a harmonization approach, integrating landcover-specific biomass maps with additional data layers, such as percent tree cover and landcover maps, to proportionally allocate estimates across different vegetation types. Santoro et al. (2021) leverage L-band SAR data to monitor forest biomass and identify carbon sinks and sources, while Global Forest Watch uses LiDAR and regional allometric equations to approximate globally (GFW, 2022). Similar work to the current research has been done by Klein et al. in urban forests, but in addition to the different setting (urban versus tropical forest), their approach differs in their use of LiDAR data to this end, rather than just pure RGB (Klein et al., 2021).

2. Materials

2.1 Study Area and Groundtruth

This research used the ReforesTree dataset, prepared by Reierson et al. (2022) for the purpose of providing a dataset that could be used in the creation of artificial intelligence oriented towards carbon accounting. The dataset comprises RGB aerial images of six agroforestry carbon offsetting sites in the central coastal region of Ecuador. Each site is approximately 0.5 ha. The forests are dry tropical forest type.

Drone images were captured in 2020 by an RGB camera from a Mavic 2 Pro drone with a resolution of 2cm per pixel. Field measurements to establish a baseline groundtruth were done by hand. This research uses the provided drone images and an associated Excel file comprising groundtruth data about diameter at breast height (DBH), aboveground biomass (AGB), bounding box shape and location, and tree species. It does not use the full preparation pipeline.

Because the data was collected in Ecuador, species names are written in Spanish and will be referred to by their Spanish names throughout this paper. Table 1 in the Appendix provides a translation table.

2.2 Computational Resources

Most work was completed on a MacBook Air with an M1 Apple Chip with 16GB of memory. For more memory intensive tasks, such as training and evaluation of the SEDD model, the HX1 High-Performance Computing (HPC) cluster provided by Research Computing Services at Imperial College London was used. Designed for GPU-accelerated workflows, the cluster is equipped with NVIDIA A100 80GB SXM GPUs.

3. Methodology

3.1. Preprocessing

Inheriting orthomosaic images cut into 4000 x 4000 pixel tiles (Reiersen et al., 2022), this

research implemented further image enhancements, considering methods for brightness and contrast adjustment, edge sharpening, and noise reduction. Specific enhancements were chosen based on combined impact on brightness, contrast, and edge intensity metrics relative to the baseline. Ultimately, Contrast Limited Adaptive Histogram Equalization (CLAHE) (Zuiderveld, 1994), Gamma Correction, and Laplacian Sharpening were applied. Figure 1 in the Appendix illustrates the applied image adjustments on an example image from the dataset.

Some of the orthomosaic tiles were largely whitespace, a by-product of the Reierson cutting technique. Those tiles with greater than 80% whitespace, eight tiles in total, were excluded from the dataset. Table 1 shows the species breakdown of the filtered dataset. Figure 2 in the Appendix shows the species breakdown in the data before and after culling.

Species Name	*Total ITCs*	*Percent ITCs*
Cacao	2021	43.54
Musacea	1504	32.41
Guaba	597	12.87
Otra Variedad (includes all other species in dataset)	428	9.22
Mango	89	1.92

Table 1. *Species Representation in Filtered Dataset.*

3.2. SEDD Architecture

This work uses a multi-task fully convolutional network known as a Single Encoder, Double Decoder (SEDD) model, inspired and developed after La Rosa et al. (2021) and Martins et al. (2021). The architecture employs a shared backbone network learning common representations for both tasks and then producing two outputs: a semantic segmentation map and a distance map (See Figure 1). Both are pixel-based. The former assigns a species classification to each pixel while the latter indicates the distance of each pixel to the nearest tree crown boundary. In the encoding phase, the network learns a general representation, and in the decoder phase, the network is able to refine task-specific representations. The models featured in the papers from which this model takes inspiration experimentally prove the benefit of a secondary distance task to provide regularization in species segmentation, particularly for sparse datasets.

3.2.1. Encoder

The shared encoder is based on ResNet18 (He et al., 2015), a popular deep convolutional neural network (DCNN) specialized for extracting hierarchical features from images at both high and low levels. A 7x7 convolution with stride 2 and a max pooling layer are initially applied to reduce dimensionality. Convolutional layers are then organized into four main sections, each with two 3x3 convolutional layers followed by batch normalization and ReLU activation. In this work, the ResNet18 model was initialized with pre-trained weights on ImageNet, and then modified by removing the fully connected layers for fine tuning on specific data. Earlier layers were retained, while the deeper layers were fine-tuned on the tree crown dataset with a lower learning rate.

3.2.2. Semantic Segmentation

For species map creation, the encoded output is fed into a DeepLabv3 decoder (Chen et al., 2018), an architecture known for excellence in semantic segmentation. Incorporating Atrous Spatial Pyramid Pooling (ASPP), a technique characterized by filters with rows or columns of zeros separating the learnable weights, allows the network to maintain a large receptive field without increasing the number of parameters or sacrificing spatial resolution. The ASPP module in this implementation includes parallel atrous convolutions with dilation rates of 12, 24, and 36.

After passing through the ASPP module, the feature map goes through 3x3 convolution, batch normalization, ReLU activation, and 1x1 convolution layers, outputting the class probabilities for each pixel in the image. The output is then passed through a softmax activation function to produce the final probability map which will be passed to the loss function.

3.2.3. Distance Regression

The distance map branch receives the ResNet-18 encoder output and passes it through a decoder composed of a 3x3 convolutional layer

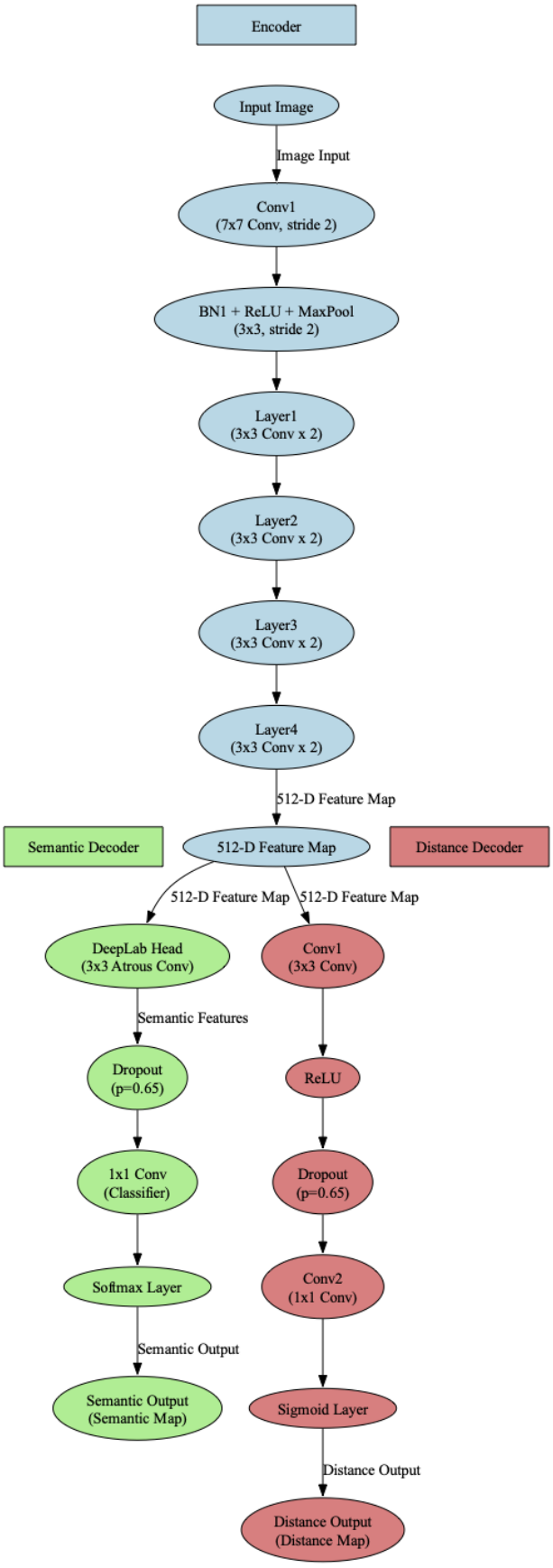

***Figure 1**. SEDD Model Architecture.*

that reduces the input feature map's dimensions, followed by a ReLU activation function and a dropout layer with a dropout rate of 0.65 to mitigate overfitting. This is followed by another 1x1 convolutional layer, which refines the feature map before applying a sigmoid activation function that outputs a continuous value between 0 and 1, representing the normalized distance for each pixel. This result is passed to the appropriate loss function, discussed in the following section.

3.2.4. Loss Calculation

This study conducted two experiments regarding the loss function for the species branch of the dual decoder. Dealing with an imbalanced dataset, segmentation loss was calculated using a modified version of categorical focal loss called Partially Weighted Categorical Focal Loss (La Rosa et al., 2021, Lin et al., 2017). This technique down weights the contribution of well-represented species, favoring the learning impact of those difficult to classify species. This loss was backpropagated through the species branch exclusively and through the shared encoder in combination with the distance loss, serving as a regulator.

Loss for the distance branch was calculated via mean squared error. This loss was backpropagated through the distance branch exclusively and through the shared encoder in combination with the species loss.

Two models were trained with the same architecture. One, henceforth known as S-SEDD (Species SEDD), favored the feedback of the species branch. In this model a technique for dealing with sparse species annotations was employed – partial loss. Partial loss only backpropagates losses based on labelled pixels (in this case, tree crowns with an associated groundtruth), and ignores unlabelled pixels (background or tree crowns without a groundtruth). This masking strategy has been shown to improve results for sparsely labeled data (Wu et al., 2018). Additionally, in the final loss passed to the shared encoder, this model favored the species loss 2:1. Whereas the other model simply adds the species and distance loss, this model multiplies the species loss by two before adding, lessening the impact of the distance regulator and focusing on the species loss as the primary output.

On the other hand, the DS-SEDD (Distance/Species SEDD) model used standard SEDD regularization, propagating at a ratio of 1:1 into the shared encoder and did not mask based on unlabelled versus labelled pixels.

3.3. Experimental Setup

The 4623 ITCs remaining after pre-processing filtration were split so that the training set had 3388 trees, the validation set had 660 trees, and the test set had 575 trees. So that the data was not made even sparser, putting trees from a singular tile into different sets, it was split in a manner that kept all trees in an individual tile together (70% of the tiles were put into the training set and the remaining 30% were split between validation and test).

The SEDD model was trained using image patches of 224 x 224 pixels. Before the patches were cropped, dual species and distance maps were created, which were then cropped in coordination with the original images (See Figure 2). Cropping happened on the fly during each epoch and transformations were applied, generating more learning images. Transformations for data augmentation included integrated horizontal and vertical flips as well as rotations (90◦, 180◦, 270◦). These transformations were also applied to the validation data.

Dropout with a rate of 0.65 was used to prevent overfitting. The model was optimized using Stochastic Gradient Descent (SGD) with a momentum of 0.9, an initial learning rate of 0.01, and a weight decay of 1e-4. The learning rate was scheduled to decay by a factor of 0.1 every 10 epochs to ensure a gradual reduction in step size as training progressed. The model was trained for 15 epochs.

For evaluation, the test data was loaded at full size, 4000 x 4000 pixels (See Figure 3 in the Appendix). Then a sliding window slid over the image, considering patches of the image one 224 x 224 window at a time (See Figure 4 in the Appendix). An overlap of 50% was used, with pixels in overlapping patches being averaged for more accurate outputs. At the end of the evaluation, the predicted species map, distance map, and probability map were saved for post-processing.

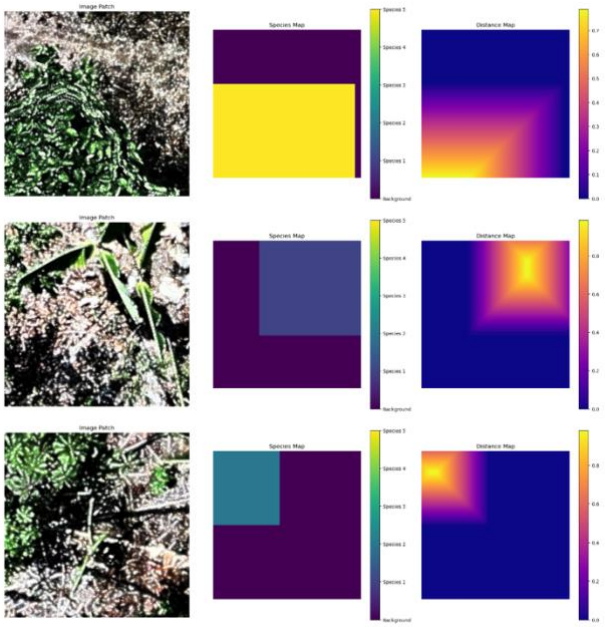

Figure 2. *Visualization of Three Image Patches, Processed with Associated Species and Distance Maps and Ready for Training in SEDD Model.*

3.4. Post-processing

Post-processing procedures took species maps from the S-SEDD and DS-SEDD models and used them to generate carbon sequestration estimates for individual trees. The distance map, while an important regularizer in the SEDD model, did not achieve the necessary accuracy for reliable use in downstream tasks such as tree crown boundary delineation and biomass estimation. Instead, the output from the SEDD model species branch was combined with DeepForest ITC bounding box predictions.

Before this, filtering of low probability pixels was performed—removing pixels where the maximum probability for a given species was less than 20%.

3.4.1 DeepForest

DeepForest is a python package trained to detect ITCs in complex forest environments using RGB aerial images (Weinstein et al., 2020). Built on a Faster R-CNN architecture, it has been trained on a variety of different forest types and geographies.

In this research, the model was fine-tuned using the same groundtruth data as the SEDD model, with precautions taken to prevent data leakage.

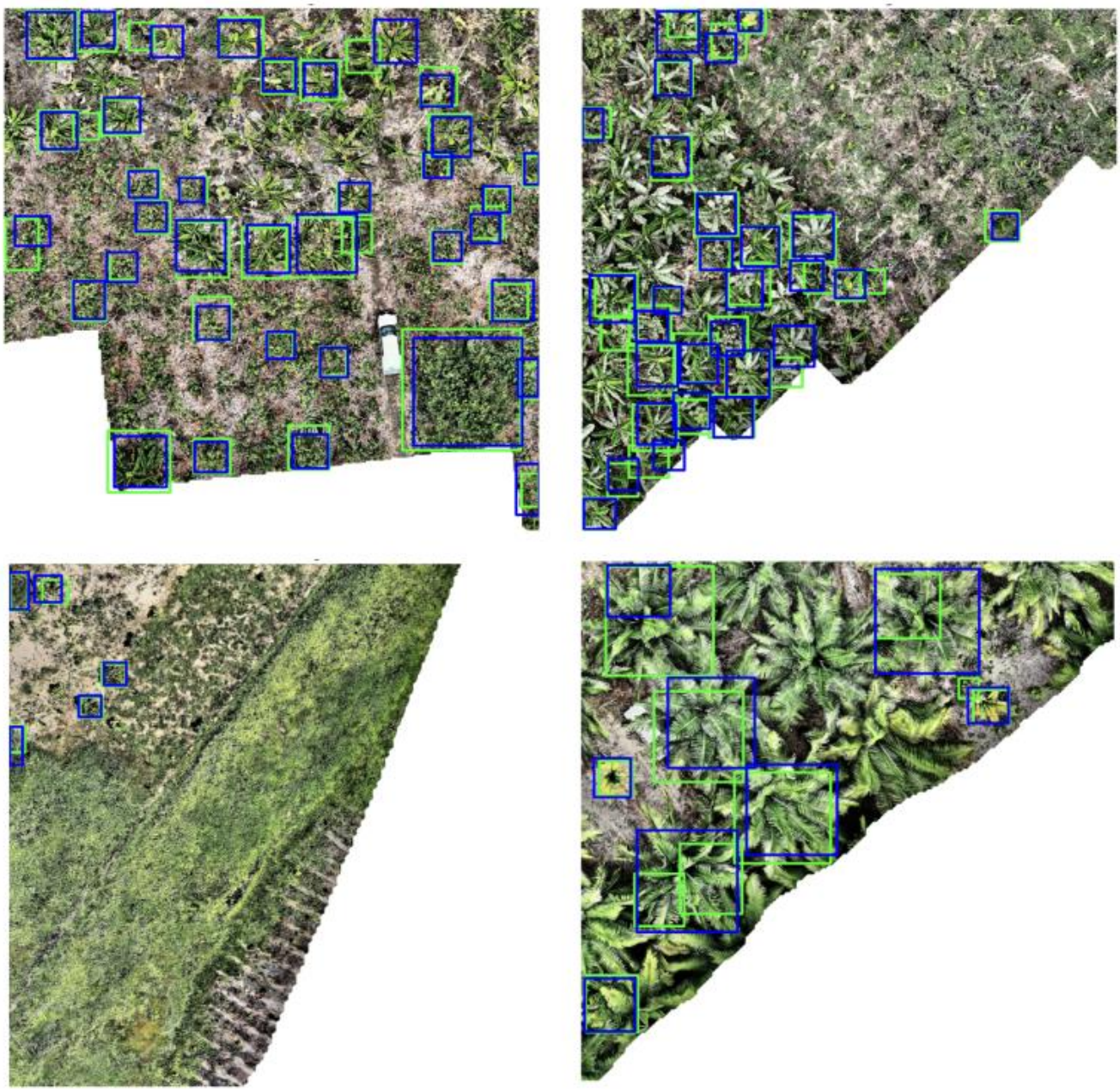

Figure 3. *Four Test Set Images with Groundtruth Bounding Boxes (Green) and DeepForest Predicted Bounding Boxes (Blue).*

The SEDD model's test set was saved into a CSV file, which was then loaded into the DeepForest training environment. This allowed for the removal of the test data from the base dataset before splitting it into standard training and validation sets (70% of data for test set and 30% for validation set).

In order for the output to be actionable in the carbon sequestration pipeline, tree crowns that aligned with the sparse groundtruth data had to be isolated from the overall bounding box predictions. DeepForest identifies all tree crowns in an image, but all trees in a given image were not groundtruthed in this dataset. If DeepForest bounding boxes were not aligned with groundtruth boxes, when moving to predict AGB, there would exist bounding boxes without associated groundtruth AGB data. If completing this process without groundtruth data, this step would not be necessary and all bounding box predictions could be used. In this research, however, the IoU was calculated for each predicted bounding box against the groundtruth data to isolate the most accurate predictions. Only those predictions with the highest IoU scores, indicating a strong match between the predicted and actual tree crown locations, were

retained for further analysis. In Figure 3, the green boxes represent the true bounding boxes and the blue boxes represent DeepForest predictions.

3.4.2. Diameter Model

The primary challenge in using ITC delineation outputs for carbon accounting, as suggested by the theoretical applications of these technologies (Lassalle et al., 2022, Luo et al., 2022), lies in the reliance on traditional allometric equations—mathematical formulas developed in dendrology to estimate the biomass, volume, or other biological characteristics of trees—on DBH. Diameter at Breast Height is the measurement of a tree's diameter at 1.37 meters above the ground. However, DBH is impossible to capture directly from aerial RGB images. While methods incorporating photogrammetry or LiDAR can generate point clouds, they primarily provide accurate height measurements from which DBH has to be inferred.

With solutions for estimating DBH still in development, this challenge remains a significant obstacle to individual-level tree carbon accounting. This in mind, this study developed a DBH prediction model based solely on species and bounding box characteristics. From the bounding box dimensions, three additional metrics were calculated: bounding box area, measuring the total area of the box in pixels; bounding box diagonal, calculating the Euclidean distance between the opposite corners of the bounding box, providing an indication of the size and shape of the tree crown; and bounding box across, which is the larger dimension between the height and width of the bounding box, representing the maximum span of the tree crown. Additionally, the tree species was one hot encoded, to be used numerically by the model.

As with the DeepForest fine-tuning, test data from SEDD model development was removed to prevent leakage. Outliers, trees with a diameter in the bottom or top 10% of the data, were removed. Additionally, there were some trees for which Reierson et al. (2022) did not gather groundtruth data on DBH. For these, they populated the data frame with the average diameter for that species. These trees were removed for the purpose of training the diameter model, but were included in the training data for other models as their AGB, bounding boxes, and species could still be groundtruthed.

The remaining data was scaled and split into a training set comprising 80% of the data and a validation set of 20%.

Four different model types were tested, the results of which can be seen in Figure 5 in the Appendix. Ultimately, a XGBoost Regressor model was selected (See Figure 6 in the Appendix). This model builds an ensemble of shallow decision trees sequentially, where each tree corrects the errors of its predecessors, allowing it to handle complex, non-linear relationships. Regularization parameters like gamma and minimum child weight help control model complexity and prevent overfitting.

The model was configured with a set of hyperparameters that included 1000 estimators, a maximum depth of 6 for each tree, a learning rate of 0.01, and subsampling and column sampling rates of 0.8 to prevent overfitting. The model also incorporated a gamma value of 0.1 to control tree splitting, and a minimum child weight of 1 to ensure leaves were formed only when sufficient data was available.

In post-processing, this model was applied to the output from combining the DeepForest model results and SEDD model results. It used predicted boxes from DeepForest and species predictions from SEDD to generate DBH predictions.

3.4.3. Custom Statistical Models and Carbon Sequestration Calculation

There are widely accepted allometric equations for common species (Segura et al., 2006), but not all species in the dataset had a previously developed custom equation. Additionally, because there was an ‘Otra Vareidad’ category, a generalized equation was needed. As such, five custom allometric statistical models were generated, one for each of the four species and one for the other species combined in this dataset.

Once again, test data and outliers were removed before testing six potential models, the results of which can be viewed Table 2 in the Appendix. The selected Generalized Additive

Model (GAM) specializes in modeling complex, non-linear relationships by applying a smooth function to the diameter feature.

This was applied to the data frame including DBH predictions, generating an estimated AGB for each tree. It is accepted that the carbon stock of a tree is approximately 50% its total biomass (Vashum and Jayakumar, 2012). And, dry tropical forests have a root-to-shoot ratio of 22% (Qi et al., 2019), meaning the below ground biomass is 22% of its above ground counterpart. Multiplying the predicted AGB by 1.22 and then dividing that total mass by 2, the carbon sequestration potential of each individual tree was calculated.

4. Results

The final result, comparing carbon sequestration predictions with groundtruth, will be the most pertinent. However, there are also intermediary results to consider throughout the prediction pipeline.

4.1. SEDD Model Results

In the Appendix (Table 3), you can see the classification accuracy and distance map mean squared error for both the S-SEDD and DS-SEDD models. F1 metrics for individual tiles can be found in Table 2.

In considering these metrics, it is important to remember the differences between the two models, as well as the differences in what the metrics measure.

The DS-SEDD model prioritizes the distance loss, backpropagating it through the model at the same ratio of impact as the species loss. The results (see Table 3 in the Appendix) confirm the hypothesis that the MSE will be more accurate for the DS-SEDD model than the S-SEDD model, meaning distance measurements are closer aligned to distance from the nearest tree crown.

On the other hand, one might expect the S-SEDD model to outperform the DS-SEDD model in species metrics, because it prioritized the species loss in training. However, the S-SEDD model also integrated masking, only backpropagating loss associated with labeled pixels. As a by-product, all background pixels are misclassified according to the comparison with groundtruth, leading to relatively high recall (the model is correctly identifying 68% of

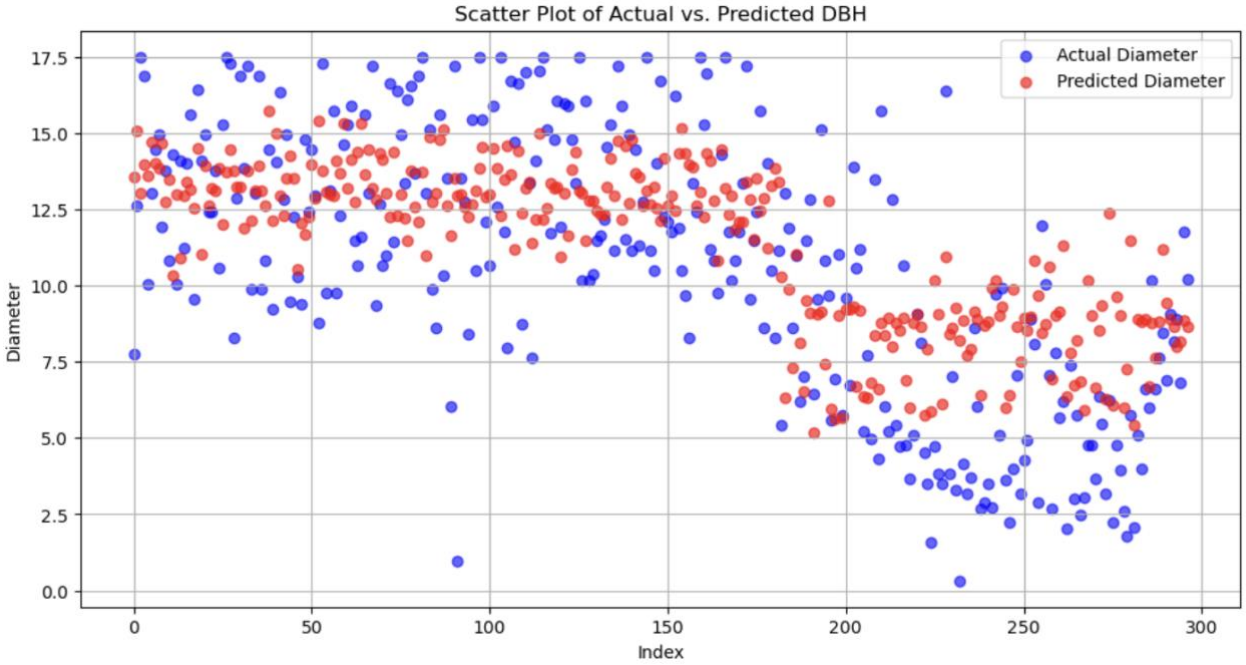

Figure 4. *Diameter Model Predictions Compared to Truth, Based on Bounding Boxes Generated from DeepForest Model and Species Classification from SEDD Model*

species pixels) but low precision (although the model is successfully labelling the species correctly, it is also labelling background pixels that aren't species as species) (See Figure 5). These issues in accuracy calculation based on masking are addressed in the use of both models in post-processing.

The DS-SEDD model, more directly comparable to other models of its kind, achieves an F1 score of 0.72, similar to industry-standard for this type of task (0.74: (Wu et al., 2020), 0.77: (Martins et al., 2021)).

4.2. Diameter and Allometric Results

The chosen diameter model had a root mean squared error (RMSE) of 2.84 on the test set established in training the model, and an RMSE of 3.27 on the outputs from the combination of the SEDD model and the DeepForest Model (see Figure 4).

While some of the other attempted diameter models achieved lower RMSE scores (see Figure 5 in the Appendix), plotting the results showed a trend of overgeneralization. With that in mind, the XGBoost model was selected for its ability to incorporate variability.

AGB statistical models proved incredibly accurate using DBH to predict AGB in a species-specific setting. The baseline model, a log-log linear regression model, achieved an R-squared score of 1 for all of the named species. For Otra Variedad, the R-squared score was 0.87.

On the other hand, the chosen Generative Additive Model still had an R-squared score of 1 for each of the named species, but achieved an R-squared score of 0.97 for the Otra Variedad category. When applied to the entire dataset, a flag was set to mark instances where there was a greater than 20% difference between actual and predicted AGB. Only 10 trees were flagged and all were of species type Otra Variedad.

4.4. AGB and Carbon Sequestration Results

Post-processing greatly improved the F1 scores for both the S-SEDD and DS-SEDD models (see Table 2). The S-SEDD Model saw an average overall increase from an F1 score of 13.9 to a score of 85.3, in large part due to the post-processing addition of background into the prediction. Post-processing improved the F1 score for the DS-SEDD model to a very similar 85.2. In challenging images, such as Flora Pluas RGB_16_11400_3800_15400_7800, where the accuracy for even the DS-SEDD model before post-processing was 47.5, a final F1 of 75.6 was achieved in both models. These improvements indicate the post-processing

Tile Name	S-SEDD		DS-SEDD	
	Before	*After*	*Before*	*After*
Carlos Vera Arteaga RGB_7_3800_11053_7800_15053	*17.62*	*98.8*	*96.7*	*99.1*
Carlos Vera Guevara RGB_10_7600_7600_11600_11600	*17.62*	*99.3*	*68.9*	*99.2*
Carlos Vera Guevara RGB_11_7600_8305_11600_12305	*17.39*	*99.4*	*88.4*	*99.4*
Flora Pluas RGB_14_7600_11578_11600_15578	*32.94*	*92.3*	*80.1*	*91.6*
Flora Pluas RGB_15_11400_0_15400_4000	*28.14*	*91.0*	*87.3*	*91.0*
Flora Pluas RGB_16_11400_3800_15400_7800	*32.94*	*75.6*	*47.5*	*75.6*
Flora Pluas RGB_9_3800_11578_7800_15578	*47.13*	*86.6*	*84.4*	*86.6*
Leonor Aspiazu RGB_14_11400_7600_15400_11600	*26.77*	*85.2*	*79.9*	*85.2*
Leonor Aspiazu RGB_2_0_7600_4000_11600	*47.36*	*78.6*	*75.9*	*78.0*
Leonor Aspiazu RGB_6_3800_7600_7800_11600	*36.38*	*60.5*	*25.4*	*59.7*
Leonor Aspiazu RGB_9_7600_3800_11600_7800	*43.47*	*78.6*	*61.6*	*78.6*
Manuel Macias RGB_5_3800_6879_7800_10879	*27.68*	*82.8*	*75.0*	*82.8*
Manuel Macias RGB_8_7600_6879_11600_10879	*46.90*	*76.1*	*44.5*	*76.1*
Manuel Macias RGB_9_9748_0_13748_4000	*26.54*	*84.1*	*81.2*	*84.1*
Nestor Macias RGB_11_7600_9024_11600_13024	*27.91*	*91.0*	*88.2*	*91.2*
Nestor Macias RGB_8_7600_0_11600_4000	*33.63*	*83.9*	*73.2*	*84.7*
Average	***13.9***	***85.3***	***72.4***	***85.2***

Table 2. *F1 Scores for Each Test Image Tile Before and After Post-Processing; Split by Model (S-SEDD and DS-SEDD.*

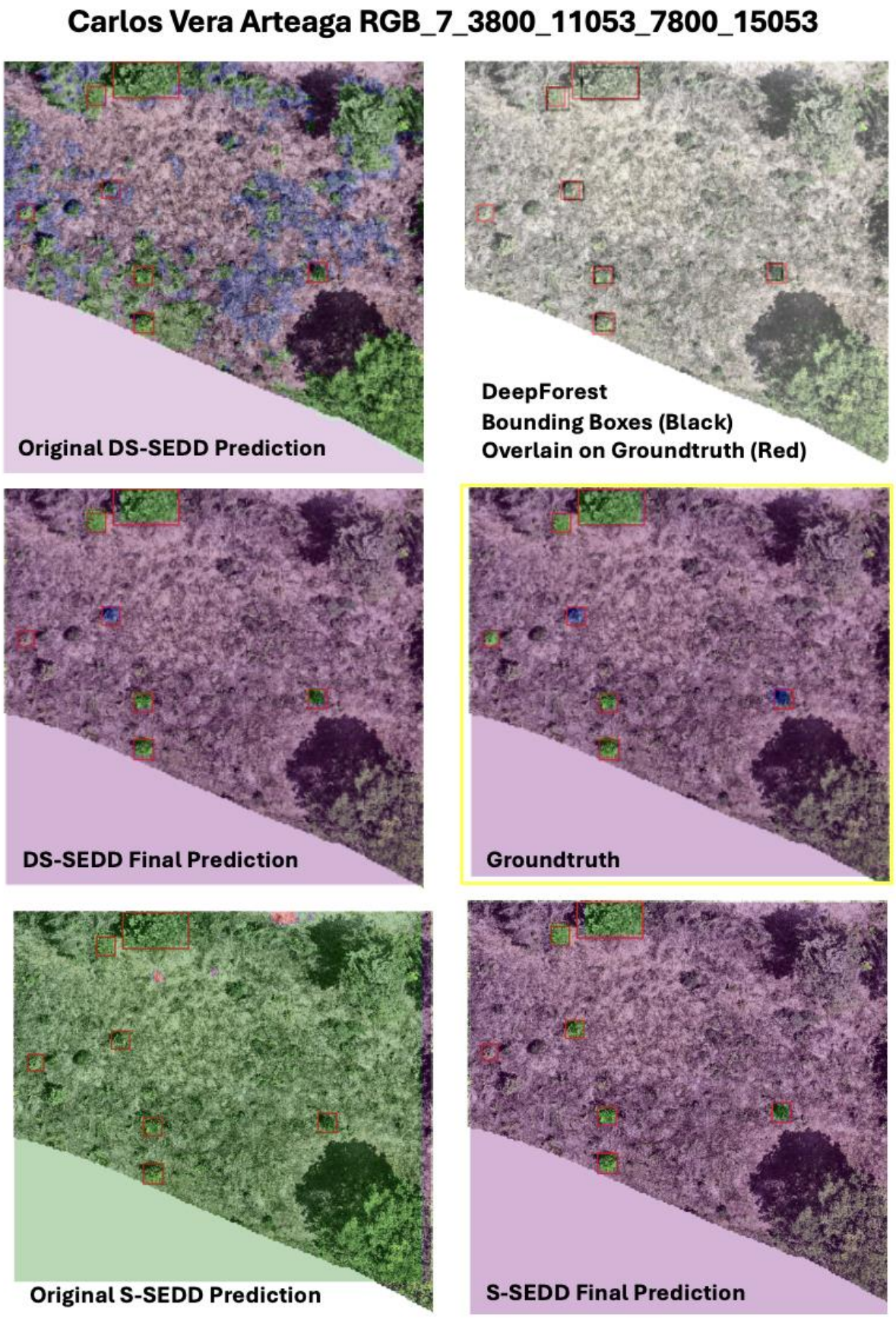

Figure 5. *Comparison of Original Model Outputs and Final Outputs (After Post-Processing); Compared to the Groundtruth and Between S-SEDD and DS-SEDD Models*

steps of combining the SEDD model output with the DeepForest output were successful in their aim of increasing the accuracy of the predictions. Figure 5 gives an example of the post-processing steps for an example test image, for both models. An additional visualization of the process on an alternate test image is available in the Appendix (Figure 7). Figure 5 demonstrates a difference in the two models. The DS-SEDD model accurately identifies a Guaba tree while the S-SEDD model mislabels it as Cacao. In the Appendix (Figure 7) the models perform equally, showing an example of Musacea/Cacao separation in a denser tile.

For both models, there tended to be a difficulty identifying species of sparser representation in the original dataset but particularly the S-SEDD model. Both models accurately identified the species of 68% of trees in the test images. This differs from the F1 score because the F1 score is pixel-based and considers correct classification of the background while the species accuracy only considers whether the predicted bounding box closest to the true bounding box was classed with the correct species. However, for just the most common species—Musacea and Cacao—accurate identification was much higher (See Table 3).

Species Name	Total # in Test Set	% Correctly Identified by S-SEDD	% Correctly Identified by DS-SEDD
Musacea	*181*	*87.8*	*91.7*
Cacao	*198*	*84.3*	*81.3*
Guaba	*50*	*0.0*	*2.0*
Mango	*3*	*0.0*	*0.0*
Otra Variedad	*51*	*0.0*	*0.0*
Total	*483*	*67.4*	*67.9*

Table 3. *Correct Classification by Bounding Box with results from S-SEDD and DS-SEDD models.*

Once the SEDD and DeepForest Model outputs were combined, AGB and carbon could be calculated using the DBH model and allometric equations. These calculations were performed considering both the situations in which species were accurately predicted and the situations in which they were not. Because the DBH and AGB models are reliant on species, results from incorrectly classed species should not be considered as pertinently as those from correctly classed species. Both are included for a robust presentation of results. The results inclusive of only correctly identified trees can be found in Table 5 while the full table is available in the Appendix (Table 4).

5. Discussion

This study illustrates the feasibility of an exciting prospect: taking an RGB aerial image of a forested area and, using a combination of deep-learning and statistical models, output an accurate estimation of individual tree-level carbon sequestration potential. Given the challenges in accurately estimating carbon storage in the past, a relative error across the test tiles of 2% could solve challenges in transparency and accuracy in the voluntary carbon market.

This pipeline was not applied to all ReforesTree data, in an effort to use the data for training and avoid leakage. This makes comparison with other strategies, which have been applied to the whole dataset, slightly challenging, but relative error can still be compared. In Table 4, courtesy of the evaluation completed by Reierson et al. (2022), you can see the predictions for the entire ReforesTree dataset using different methods of AGB prediction. The original data relates to AGB, not carbon, but as carbon is simply a linear transformation of AGB the relative error remains the same.

ReforesTree Site No.	*GFW 2019*	*Spawn 2020*	*Santoro 2021*	*Reierson 2022*
1	10.3	9.5	0.75	0.13
2	5.6	5.8	0.2	0.46
3	1.5	2.3	0.9	0.5
4	0.8	15.4	1.4	0.27
5	4.2	4.1	0.0	0.27
6	1.5	1.91	0.33	0.25
Total	4.0	5.25	0.34	0.02

Table 4. *Relative Error by Other Reports in Predicted AGB.*

The only study that approaches the 2% relative error ultimately achieved by this project is Reierson et al. and their model requires manually collected metrics for Diameter at Breast Height and Species. Even the relative error for the species agnostic calculations (0.32) approach the relative error of the second best AGB prediction method (Santoro et al., 2021), a study which used satellite L-band observations

Tile Name	*DS-SEDD Model*				*S-SEDD Model*			
Controlled for Species Matching	Actual Carbon	Predicted Carbon	Absolute Difference	Relative Difference	Actual Carbon	Predicted Carbon	Absolute Difference	Relative Difference
Carlos Vera Arteaga RGB_7_3800_11053_7800_15053.png	46.16	36.73	9.43	0.2	44.77	28.33	16.44	0.37
Carlos Vera Guevara RGB_10_7600_7600_11600_11600.png	16.6	15.84	0.77	0.05	16.6	15.84	0.77	0.05
Carlos Vera Guevara RGB_11_7600_8305_11600_12305.png	6.64	6.74	0.09	0.01	6.64	6.74	0.09	0.01
Flora Pluas RGB_14_7600_11578_11600_15578.png	104.34	94.44	9.91	0.09	104.34	94.44	9.91	0.09
Flora Pluas RGB_15_11400_0_15400_4000.png	88.1	68.13	19.97	0.23	77.32	59.63	17.68	0.23
Flora Pluas RGB_16_11400_3800_15400_7800.png	157.86	131.07	26.79	0.17	151.21	126.18	25.03	0.17
Flora Pluas RGB_9_3800_11578_7800_15578.png	93.55	71.39	22.16	0.24	98.03	73.82	24.2	0.25
Leonor Aspiazu RGB_14_11400_7600_15400_11600.png	16.69	20.84	4.16	0.25	16.69	20.84	4.16	0.25
Leonor Aspiazu RGB_2_0_7600_4000_11600.png	87.63	113.82	26.19	0.3	85.4	110.22	24.83	0.29
Leonor Aspiazu RGB_6_3800_7600_7800_11600.png	134.21	147.01	12.8	0.1	134.21	147.01	12.8	0.1
Leonor Aspiazu RGB_9_7600_3800_11600_7800.png	168.7	171.92	3.23	0.02	168.7	171.92	3.23	0.02
Manuel Macias RGB_5_3800_6879_7800_10879.png	17.85	18.28	0.42	0.02	17.85	18.28	0.42	0.02
Manuel Macias RGB_8_7600_6879_11600_10879.png	16.29	24.13	7.84	0.48	16.29	24.13	7.84	0.48
Manuel Macias RGB_9_9748_0_13748_4000.png	0.53	2.95	2.42	4.6	0.53	2.95	2.42	4.6
Nestor Macias RGB_11_7600_9024_11600_13024.png	106.47	99.9	6.57	0.06	109.8	102.34	7.46	0.07
Nestor Macias RGB_8_7600_0_11600_4000.png	160.42	166.26	5.84	0.04	153.05	162.52	9.47	0.06
Total	**1222.04**	**1189.45**	**32.59**	**0.02**	**1201.4**	**1165.2**	**36.2**	**0.03**

Table 5. *Carbon Sequestration Results for Each Tile in the Test Set, Controlled for Only Those Trees Where the Predicted Species Matched the Actual Species*

and did not consider the individual tree level. It was exactly these types of regional averages (also employed by the other two comparative studies (GFW, 2022, Spawn et al., 2020)) that were identified as causing the gross overestimation of carbon potential underlying the world's carbon credits (Badgley et al., 2022).

The solution proposed by the current study is lightweight in its data requirements, only requiring RGB imagery, and demonstrates an accuracy in predicting carbon sequestration methods outperforming even those studies which require more data.

6. Limitations and Future Work

This project used RGB aerial data, in large part because of its availability in lower-income areas. However, there are more sophisticated techniques that could have been employed if using multispectral or LiDAR data, particularly as it relates to DBH approximation.

Additionally, because the evaluation of the SEDD model required the use of a high-performance computing (HPC) cluster, recreating this pipeline could pose accessibility challenges in lower-income areas. While there is no need for manual data collection, a huge benefit to the scalability of this solution, HPCs are not widely available. With that in mind, future work may look to creating a sleeker species segmentation model which could be trained more quickly and evaluated on less powerful computing infrastructure. When considering improvements to the species segmentation model, there is also the obvious challenge of sparse and unbalanced data. Future work may consider more data augmentation techniques to address class imbalance or models particularly trained on detecting an individual species and leveraged in parallel.

Finally, this model was only trained on a dry tropical forest type. Conducting similar work in

different geographical regions or forest types would advance this proof of concept toward actionable implementation. Developing a product based on this pipeline, where a user could simply submit their image and receive tree-level carbon accounting metrics via a user-friendly interface, would also be a crucial step in making this technology useful for the voluntary global carbon market.

Resources

BADGLEY, G., FREEMAN, J., HAMMAN, J. J., HAYA, B., TRUGMAN, A. T., ANDEREGG, W. R. L. & CULLENWARD, D. 2022. Systematic over-crediting in California's forest carbon offsets program. *Global Change Biology,* 28**,** 1433-1445.

CHEN, L. C., PAPANDREOU, G., KOKKINOS, I., MURPHY, K. & YUILLE, A. L. 2018. DeepLab: Semantic Image Segmentation with Deep Convolutional Nets, Atrous Convolution, and Fully Connected CRFs. *IEEE Transactions on Pattern Analysis and Machine Intelligence,* 40**,** 834-848.

FAO 2020. Global Forest Resources Assessment 2020.

FASSNACHT, F. E., LATIFI, H., STEREńCZAK, K., MODZELEWSKA, A., LEFSKY, M., WASER, L. T., STRAUB, C. & GHOSH, A. 2016. Review of studies on tree species classification from remotely sensed data. *Remote Sensing of Environment,* 186**,** 64-87.

FERREIRA, M. P., ALMEIDA, D. R. A. D., PAPA, D. D. A., MINERVINO, J. B. S., VERAS, H. F. P., FORMIGHIERI, A., SANTOS, C. A. N., FERREIRA, M. A. D., FIGUEIREDO, E. O. & FERREIRA, E. J. L. 2020. Individual tree detection and species classification of Amazonian palms using UAV images and deep learning. *Forest Ecology and Management,* 475**,** 118397.

G. BRAGA, J. R., PERIPATO, V., DALAGNOL, R., P. FERREIRA, M., TARABALKA, Y., O. C. ARAGãO, L. E., F. DE CAMPOS VELHO, H., SHIGUEMORI, E. H. & WAGNER, F. H. 2020. Tree Crown Delineation Algorithm Based on a Convolutional Neural Network. *Remote Sensing* [Online], 12.

GFW 2022. Global Forest Watch Dataset. Global Forest Watch.

HE, K., ZHANG, X., REN, S. & SUN, J. 2015. Deep Residual Learning for Image Recognition. *2016 IEEE Conference on Computer Vision and Pattern Recognition (CVPR)***,** 770-778.

IPCC 2022. Land–climate interactions. *In:* INTERGOVERNMENTAL PANEL ON CLIMATE, C. (ed.) *Climate Change and Land: IPCC Special Report on Climate Change, Desertification, Land Degradation, Sustainable Land Management, Food Security, and Greenhouse Gas Fluxes in Terrestrial Ecosystems.* Cambridge: Cambridge University Press.

KLEIN, L., ZHOU, W. & ALBRECHT, C. 2021. *Quantification of Carbon Sequestration in Urban Forests*.

KORZNIKOV, K. A., KISLOV, D. E., ALTMAN, J., DOLEŽAL, J., VOZMISHCHEVA, A. S. & KRESTOV, P. V. 2021. Using U-Net-Like Deep Convolutional Neural Networks for Precise Tree Recognition in Very High Resolution RGB (Red, Green, Blue) Satellite Images. *Forests* [Online], 12.

LA ROSA, L. E. C., SOTHE, C., FEITOSA, R. Q., DE ALMEIDA, C. M., SCHIMALSKI, M. B. & OLIVEIRA, D. A. B. 2021. Multi-task fully convolutional network for tree species mapping in dense forests using small training hyperspectral data. *ISPRS Journal of Photogrammetry and Remote Sensing,* 179**,** 35-49.

LASSALLE, G., FERREIRA, M. P., LA ROSA, L. E. C. & DE SOUZA FILHO, C. R. 2022. Deep learning-based individual tree crown delineation in mangrove forests using very-high-resolution satellite imagery. *ISPRS Journal of*

Photogrammetry and Remote Sensing, 189**,** 220-235.

LIN, T.-Y., GOYAL, P., GIRSHICK, R., HE, K. & DOLLAR, P. 2017. Focal Loss for Dense Object Detection. *2017 IEEE International Conference on Computer Vision (ICCV).* IEEE Computer Society.

LUO, M., TIAN, Y., ZHANG, S., HUANG, L., WANG, H., LIU, Z. & YANG, L. 2022. Individual Tree Detection in Coal Mine Afforestation Area Based on Improved Faster RCNN in UAV RGB Images. *Remote Sensing* [Online], 14.

MARTINS, G. B., LA ROSA, L. E. C., HAPP, P. N., FILHO, L. C. T. C., SANTOS, C. J. F., FEITOSA, R. Q. & FERREIRA, M. P. 2021. Deep learning-based tree species mapping in a highly diverse tropical urban setting. *Urban Forestry & Urban Greening,* 64**,** 127241.

QI, Y., WEI, W., CHEN, C. & CHEN, L. 2019. Plant root-shoot biomass allocation over diverse biomes: A global synthesis. *Global Ecology and Conservation,* 18**,** e00606.

REIERSEN, G., DAO, D., LüTJENS, B., KLEMMER, K., AMARA, K., STEINEGGER, A., ZHANG, C. & ZHU, X. 2022. ReforesTree: A Dataset for Estimating Tropical Forest Carbon Stock with Deep Learning and Aerial Imagery. *Proceedings of the AAAI Conference on Artificial Intelligence,* 36**,** 12119-12125.

SANTORO, M., CARTUS, O., CARVALHAIS, N., ROZENDAAL, D. M. A., AVITABILE, V., ARAZA, A., DE BRUIN, S., HEROLD, M., QUEGAN, S., RODRíGUEZ-VEIGA, P., BALZTER, H., CARREIRAS, J., SCHEPASCHENKO, D., KORETS, M., SHIMADA, M., ITOH, T., MORENO MARTíNEZ, Á., CAVLOVIC, J., CAZZOLLA GATTI, R., DA CONCEIçãO BISPO, P., DEWNATH, N., LABRIèRE, N., LIANG, J., LINDSELL, J., MITCHARD, E. T. A., MOREL, A., PACHECO PASCAGAZA, A. M., RYAN, C. M., SLIK, F., VAGLIO LAURIN, G., VERBEECK, H., WIJAYA, A. & WILLCOCK, S. 2021. The global forest above-ground biomass pool for 2010 estimated from high-resolution satellite observations. *Earth Syst. Sci. Data,* 13**,** 3927-3950.

SEGURA, M., KANNINEN, M. & SUáREZ, D. 2006. Allometric models for estimating aboveground biomass of shade trees and coffee bushes grown together. *Agroforestry Systems,* 68**,** 143-150.

SHI, H., TIAN, H., LANGE, S., YANG, J., PAN, S., FU, B. & REYER, C. P. O. 2021. Terrestrial biodiversity threatened by increasing global aridity velocity under high-level warming. *Proceedings of the National Academy of Sciences,* 118**,** e2015552118.

SOTHE, C., DALPONTE, M., ALMEIDA, C. M., SCHIMALSKI, M. B., LIMA, C. L., LIESENBERG, V., MIYOSHI, G. T. & TOMMASELLI, A. M. 2019. Tree Species Classification in a Highly Diverse Subtropical Forest Integrating UAV-Based Photogrammetric Point Cloud and Hyperspectral Data. *Remote Sensing* [Online], 11.

SPAWN, S. A., SULLIVAN, C. C., LARK, T. J. & GIBBS, H. K. 2020. Harmonized global maps of above and belowground biomass carbon density in the year 2010. *Scientific Data,* 7**,** 112.

SUN, W. & LIU, X. 2019. Review on carbon storage estimation of forest ecosystem and applications in China. *Forest Ecosystems,* 7**,** 4.

VASHUM, K. T. & JAYAKUMAR, S. 2012. Methods to estimate above-ground biomass and carbon stock in natural forests-a review. *Journal of Ecosystem & Ecography,* 2**,** 1-7.

WEINSTEIN, B. G., MARCONI, S., AUBRY-KIENTZ, M., VINCENT, G., SENYONDO, H. & WHITE, E. P. 2020. DeepForest: A Python package for RGB deep learning tree crown delineation. *Methods in Ecology and Evolution,* 11**,** 1743-1751.

WU, J., YANG, G., YANG, H., ZHU, Y., LI, Z., LEI, L. & ZHAO, C. 2020. Extracting apple tree crown information from remote imagery using deep learning. *Computers and Electronics in Agriculture,* 174**,** 105504.

WU, W., QI, H., RONG, Z., LIU, L. & SU, H. 2018. Scribble-Supervised Segmentation of Aerial Building Footprints Using Adversarial Learning. *IEEE Access,* PP**,** 1-1.

ZHANG, B., ZHAO, L. & ZHANG, X. 2020. Three-dimensional convolutional neural network model for tree species classification using airborne hyperspectral images. *Remote Sensing of Environment,* 247**,** 111938.

ZUIDERVELD, K. 1994. Contrast limited adaptive histogram equalization. *Graphics gems IV.* Academic Press Professional, Inc.

Appendix

Table 1. *Species Name Translations*

Spanish Name	*English Name*
Cacao	Cacao
Musacea	Musaceae (more commonly known as the banana tree)
Guaba	Guava
Mango	Mango
Otra Variedad	Other Variety

Figure 1. *A selected image tile from the ReforesTree dataset before and after image enhancements are applied.*

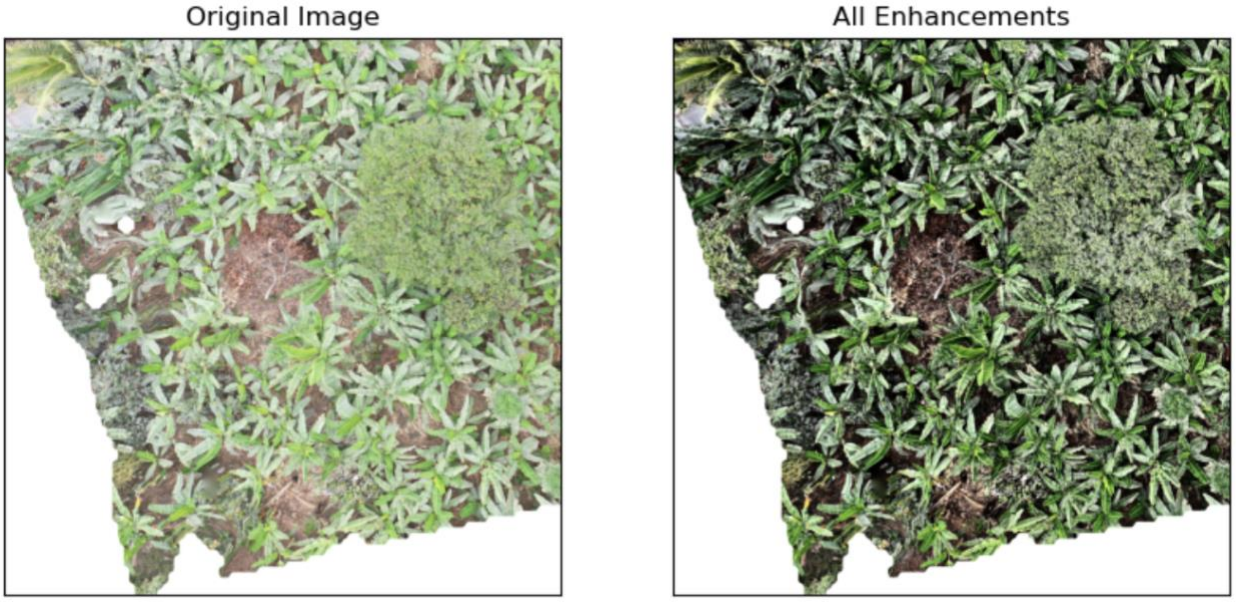

Figure 2. *Species Representation in Dataset Before and After Filtering*

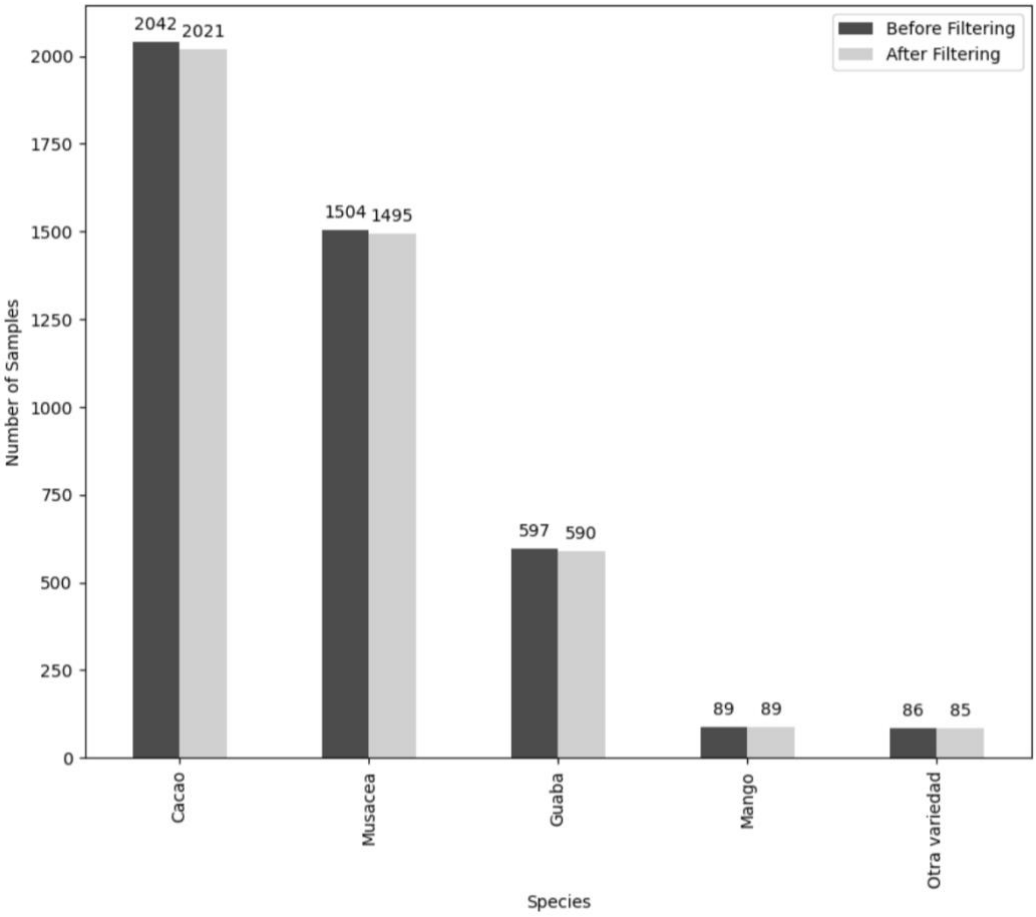

Figure 3. *An Example Test Image with Associated Species and Distance Maps; Ready for Evaluation.*

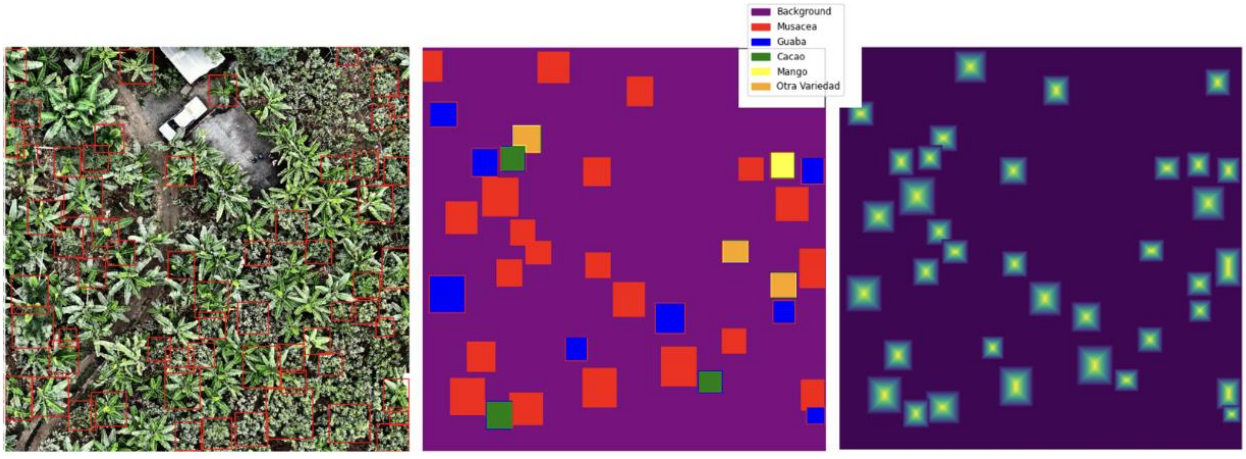

Figure 4. *Visualization of Sliding Window Movement Over Example Image with 50% Overlap.*

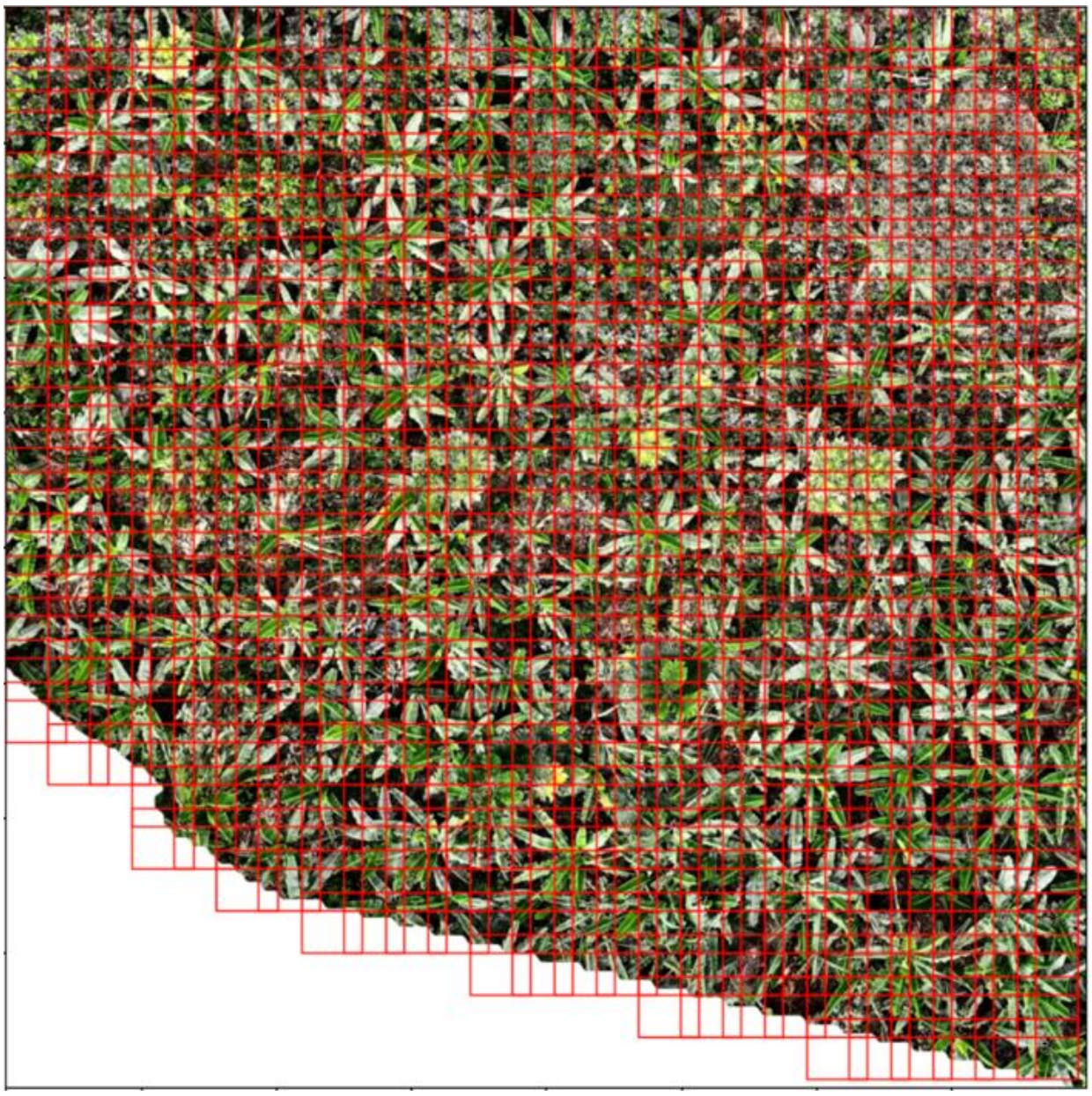

Figure 5. *Comparison of DBH Models*

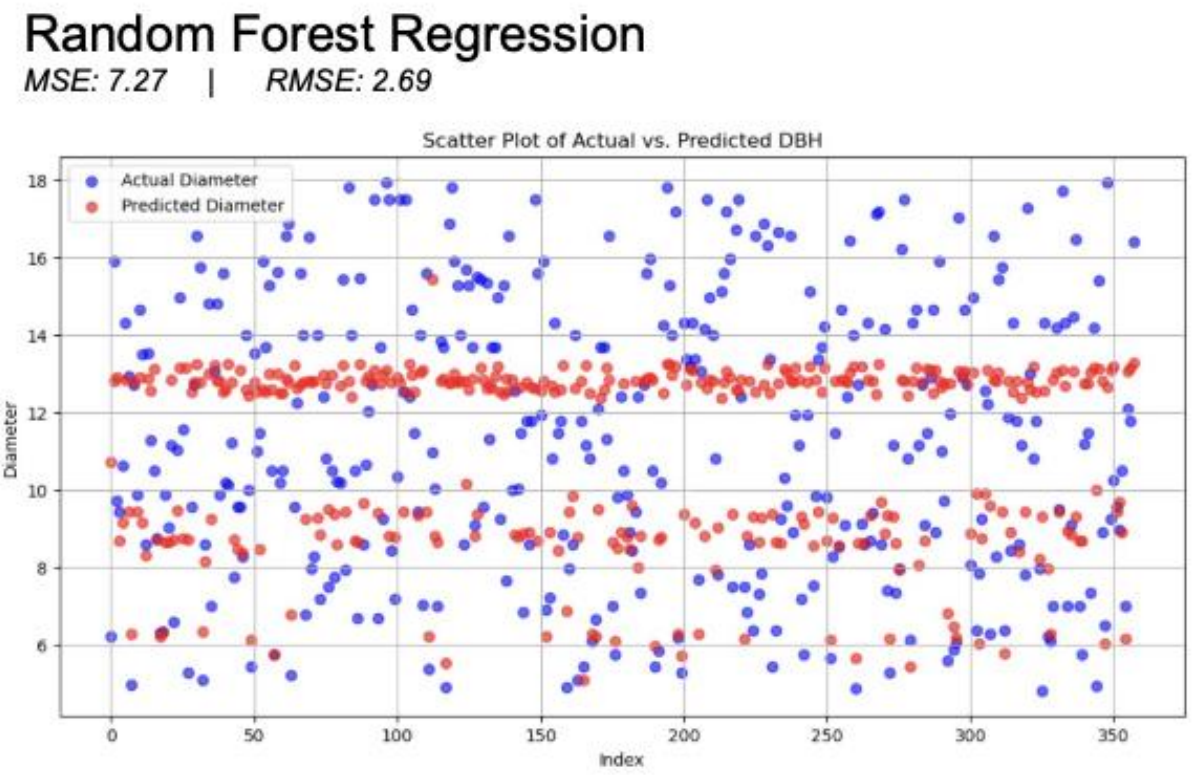

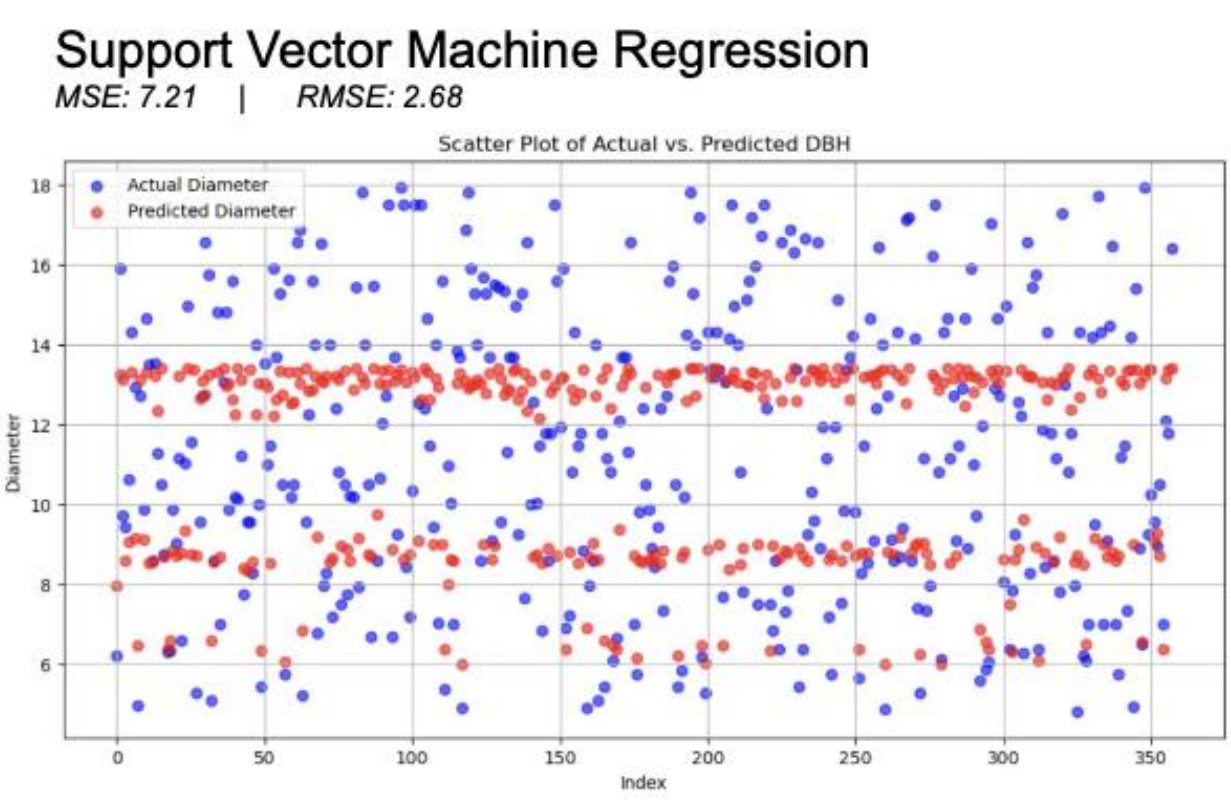

Complex Neural Network

MSE: 7.55 | RMSE: 2.75

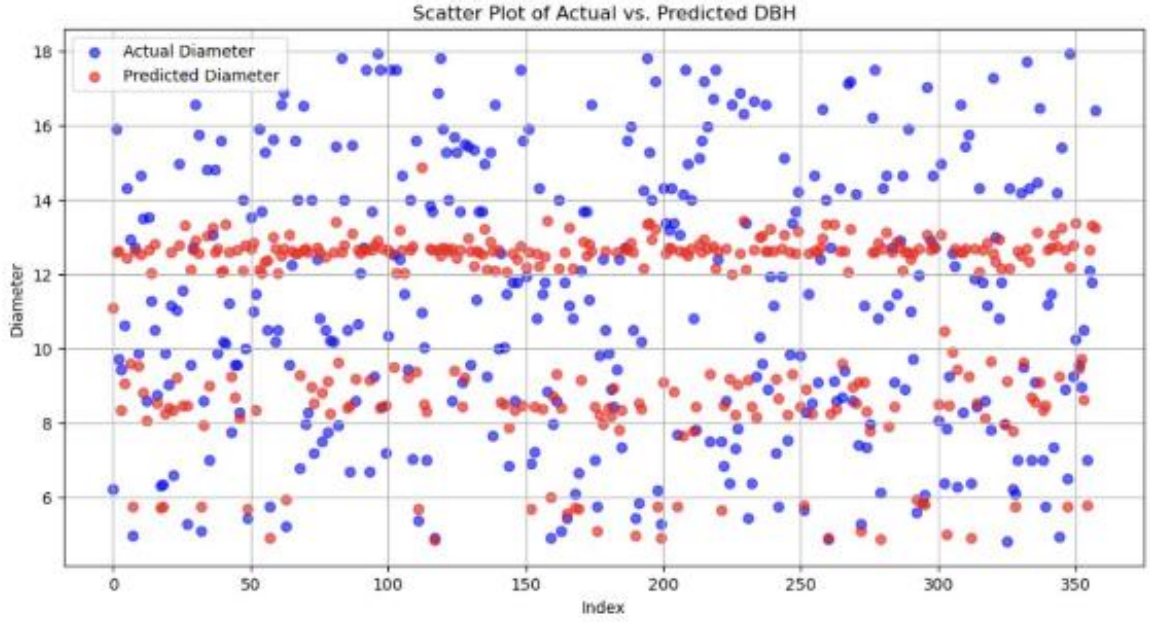

XGBoost [SELECTED MODEL]

MSE: 8.07 | RMSE: 2.84

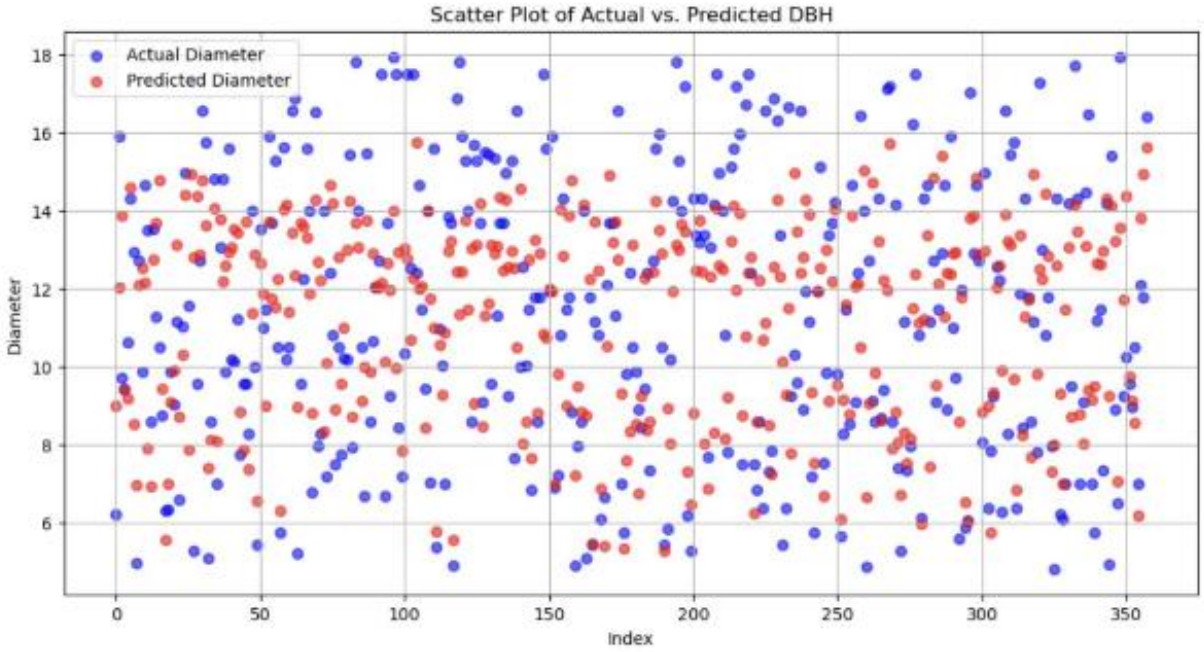

Figure 6. *Diameter Model Architecture (XGBoost Regressor)*

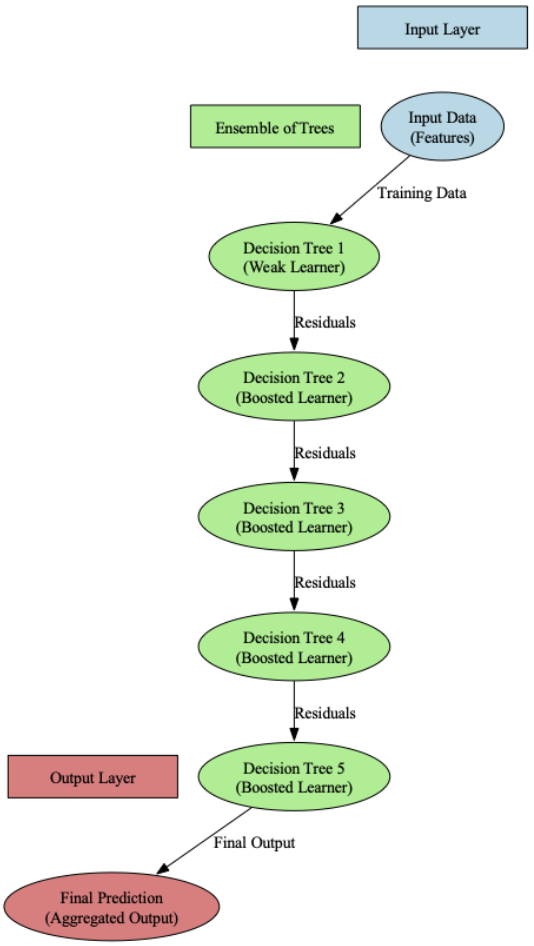

Table 2. *Comparison of R-Squared Scores from Statistical Allometric Models*

	Log Log	*Linear*	*Exponential*	*Logarithmic*	*Polynomial*	*GAM*
Musacea	1.0	0.99	0.99	0.97	1.0	1.0
Cacao	1.0	0.99	0.98	0.95	1.0	1.0
Guaba	1.0	0.97	0.98	0.93	1.0	1.0
Mango	1.0	1.0	1.0	0.99	1.0	1.0
Otra Variedad	0.87	0.86	0.92	0.71	0.93	0.98

Table 3. *Accuracy Metrics from SEDD models before post-processing (Section 3.4)*

		S-SEDD	*DS-SEDD*
Species	F1	31.90	72.40
	Precision	68.43	85.73
	Recall	20.80	63.74
Distance	MSE	0.0515	0.0379

Figure 7. *Comparison of Original Model Outputs and Final Outputs (After Post-Processing); Compared to the Groundtruth and Between S-SEDD and DS-SEDD Models*

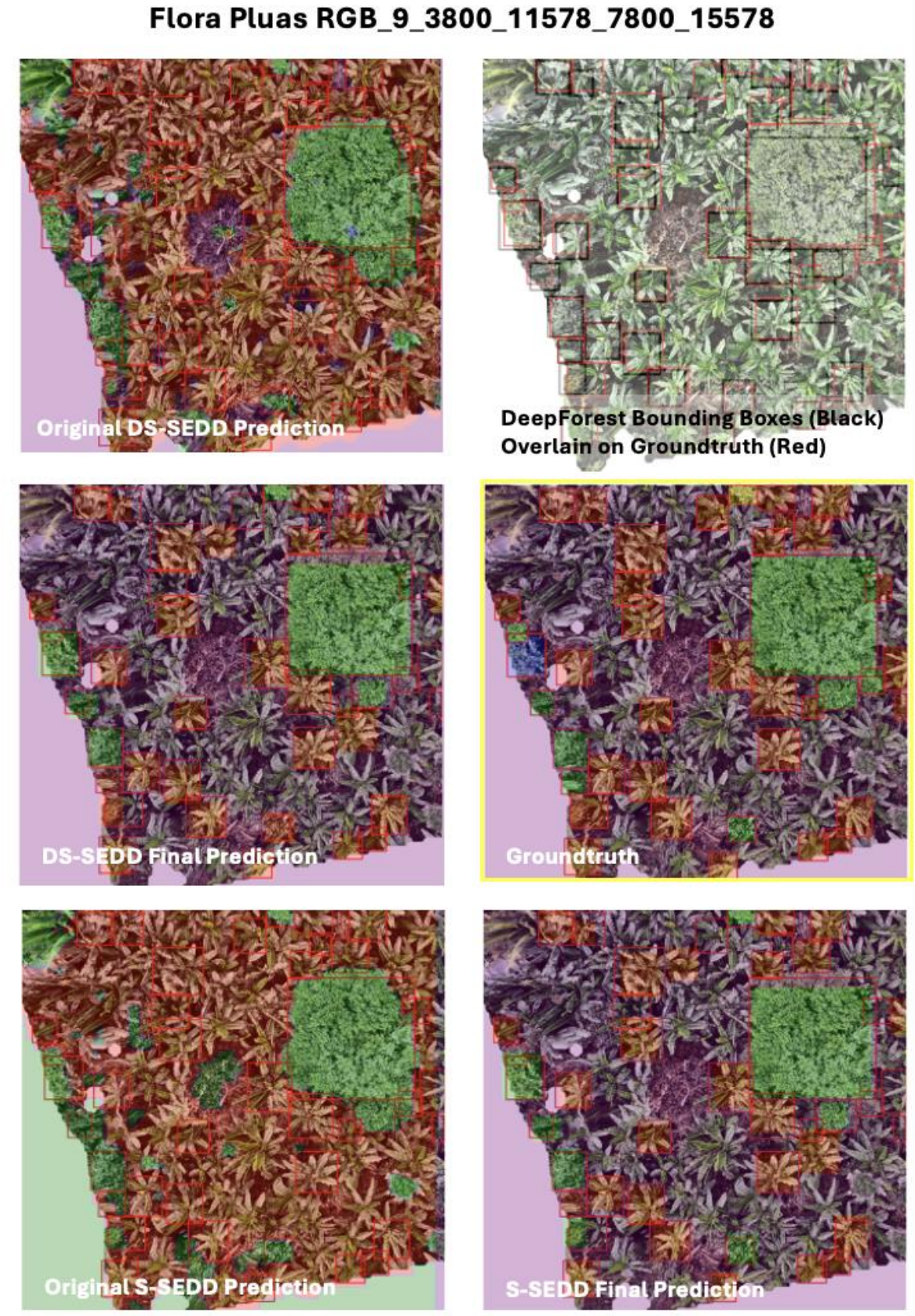

Table 4. *Carbon Sequestration Results for Each Tile in the Test Set, Comparison Between Controlling for Species and Whole Dataset*

Tile Name	*DS-SEDD Model*				*S-SEDD Model*			
Controlled for Species Matching	Actual Carbon	Predicted Carbon	Absolute Difference	Relative Difference	Actual Carbon	Predicted Carbon	Absolute Difference	Relative Difference
Carlos Vera Arteaga RGB_7_3800_11053_7800_15053.png	46.16	36.73	9.43	0.2	44.77	28.33	16.44	0.37
Carlos Vera Guevara RGB_10_7600_7600_11600_11600.png	16.6	15.84	0.77	0.05	16.6	15.84	0.77	0.05
Carlos Vera Guevara RGB_11_7600_8305_11600_12305.png	6.64	6.74	0.09	0.01	6.64	6.74	0.09	0.01
Flora Pluas RGB_14_7600_11578_11600_15578.png	104.34	94.44	9.91	0.09	104.34	94.44	9.91	0.09
Flora Pluas RGB_15_11400_0_15400_4000.png	88.1	68.13	19.97	0.23	77.32	59.63	17.68	0.23
Flora Pluas RGB_16_11400_3800_15400_7800.png	157.86	131.07	26.79	0.17	151.21	126.18	25.03	0.17
Flora Pluas RGB_9_3800_11578_7800_15578.png	93.55	71.39	22.16	0.24	98.03	73.82	24.2	0.25
Leonor Aspiazu RGB_14_11400_7600_15400_11600.png	16.69	20.84	4.16	0.25	16.69	20.84	4.16	0.25
Leonor Aspiazu RGB_2_0_7600_4000_11600.png	87.63	113.82	26.19	0.3	85.4	110.22	24.83	0.29
Leonor Aspiazu RGB_6_3800_7600_7800_11600.png	134.21	147.01	12.8	0.1	134.21	147.01	12.8	0.1
Leonor Aspiazu RGB_9_7600_3800_11600_7800.png	168.7	171.92	3.23	0.02	168.7	171.92	3.23	0.02
Manuel Macias RGB_5_3800_6879_7800_10879.png	17.85	18.28	0.42	0.02	17.85	18.28	0.42	0.02
Manuel Macias RGB_8_7600_6879_11600_10879.png	16.29	24.13	7.84	0.48	16.29	24.13	7.84	0.48
Manuel Macias RGB_9_9748_0_13748_4000.png	0.53	2.95	2.42	4.6	0.53	2.95	2.42	4.6
Nestor Macias RGB_11_7600_9024_11600_13024.png	106.47	99.9	6.57	0.06	109.8	102.34	7.46	0.07
Nestor Macias RGB_8_7600_0_11600_4000.png	160.42	166.26	5.84	0.04	153.05	162.52	9.47	0.06
Total	**1222.04**	**1189.45**	**32.59**	**0.02**	**1201.4**	**1165.2**	**36.2**	**0.03**
Whole Test Dataset – Not Controlled for Species Matching								
Carlos Vera Arteaga RGB_7_3800_11053_7800_15053.png	58.71	50.56	-8.15	0.14	58.71	34.73	-23.97	0.41
Carlos Vera Guevara RGB_10_7600_7600_11600_11600.png	62.98	23.82	-39.16	0.62	62.98	23.82	-39.16	0.62
Carlos Vera Guevara RGB_11_7600_8305_11600_12305.png	83.24	25.23	-58.01	0.70	83.24	25.23	-58.01	0.70
Flora Pluas RGB_14_7600_11578_11600_15578.png	112.19	95.00	-17.19	0.15	112.19	95.00	-17.19	0.15
Flora Pluas RGB_15_11400_0_15400_4000.png	169.07	79.50	-89.57	0.53	169.07	84.34	-84.73	0.50
Flora Pluas RGB_16_11400_3800_15400_7800.png	436.79	168.71	-268.08	0.61	436.79	178.07	-258.72	0.59
Flora Pluas RGB_9_3800_11578_7800_15578.png	159.10	88.39	-70.71	0.44	159.10	90.61	-68.49	0.43
Leonor Aspiazu RGB_14_11400_7600_15400_11600.png	28.91	32.66	3.75	0.13	28.91	32.66	3.75	0.13
Leonor Aspiazu RGB_2_0_7600_4000_11600.png	235.12	193.03	-42.09	0.18	235.12	204.61	-30.51	0.13
Leonor Aspiazu RGB_6_3800_7600_7800_11600.png	335.81	286.59	-49.21	0.15	335.81	288.95	-46.85	0.14
Leonor Aspiazu RGB_9_7600_3800_11600_7800.png	285.42	223.47	-61.96	0.22	285.42	223.47	-61.96	0.22
Manuel Macias RGB_5_3800_6879_7800_10879.png	41.27	41.32	0.05	0.00	41.27	41.32	0.05	0.00

Manuel Macias RGB_8_7600_6879_11600_10879.png	77.36	75.16	-2.20	0.03	77.36	75.16	-2.20	0.03
Manuel Macias RGB_9_9748_0_13748_4000.png	21.73	17.21	-4.52	0.21	21.73	17.21	-4.52	0.21
Nestor Macias RGB_11_7600_9024_11600_13024.png	154.21	113.73	-40.47	0.26	154.21	118.31	-35.89	0.23
Nestor Macias RGB_8_7600_0_11600_4000.png	307.34	212.49	-94.85	0.31	307.34	214.95	-92.39	0.30
Total	**2569.25**	**1726.87**	**842.38**	**0.32**	**2569.25**	**1748.44**	**820.81**	**0.32**